

# Hydrogen bonding and coordination in normal and supercritical water from X-ray inelastic scattering

Patrick H.-L. Sit,<sup>1</sup> Christophe Bellin,<sup>2</sup> Bernardo Barbiellini,<sup>3</sup> D.

Testemale,<sup>4</sup> J.-L. Hazemann,<sup>4</sup> T. Buslaps,<sup>5</sup> Nicola Marzari,<sup>6</sup> Abhay Shukla<sup>2</sup>

<sup>1</sup>*Department of Physics, Massachusetts Institute of Technology, Cambridge, MA 02139, USA*

<sup>2</sup>*Institut de Minéralogie et de Physique des Milieux Condensés,*

*Université Pierre et Marie Curie, case 115,*

*4 place Jussieu 75252 Paris Cedex 05, France*

<sup>3</sup>*Department of Physics, Northeastern University, Boston, MA 02115, USA*

<sup>4</sup>*Laboratoire de Cristallographie, UPR 5031, 26 Avenue des Martyrs,*

*Boite Postale 166, 38042 Grenoble Cedex 9, France*

<sup>5</sup>*European Synchrotron Radiation Facility,*

*BP 220, F-38043 Grenoble Cedex, France*

<sup>6</sup>*Department of Materials Science and Engineering,*

*Massachusetts Institute of Technology, Cambridge, MA 02139, USA*

(Dated: March 23, 2022)

## Abstract

A direct measure of hydrogen bonding in water under conditions ranging from the normal state to the supercritical regime is derived from the Compton scattering of inelastically-scattered X-rays. First, we show that a measure of the number of electrons  $n_e$  involved in hydrogen bonding at varying thermodynamic conditions can be directly obtained from Compton profile differences. Then, we use first-principles simulations to provide a connection between  $n_e$  and the number of hydrogen bonds  $n_{HB}$ . Our study shows that over the broad range studied the relationship between  $n_e$  and  $n_{HB}$  is linear, allowing for a direct experimental measure of bonding and coordination in water. In particular, the transition to supercritical state is characterized by a sharp increase in the number of water monomers, but also displays a significant number of residual dimers and trimers.

The complexity of the phase diagram of water and its relevance to many physical, chemical and biological processes is to a large extent related to the presence of hydrogen bonds [1]. Over the years, different methods have been used to investigate the structure and dynamics of water [2]; nevertheless, many fascinating questions still remain. Hydrogen bonding and coordination in disordered phases, most notably in the liquid, are the subject of intense study and the average number of hydrogen bonds ( $n_{HB}$ ) in water has recently become a subject of controversy [3, 4]. X-ray absorption spectroscopy (XAS) [3] in water and ice indicated that the liquid contains significantly more broken hydrogen bonds than previously thought, but these conclusions have been questioned [4, 5]. The degree of persistence of hydrogen bonding in the region beyond the critical point is also an interesting question [6]. Several works report on residual hydrogen bonding in supercritical water [2, 7]. The number of hydrogen bonds per molecule  $n_{HB}$  is a concept of some ambiguity since it depends on geometric definitions. The connectivity of the hydrogen bonded network has also been recently studied in terms of electronic signatures [8] highlighting the presence of a fast electronic bond dynamics and reorganization.

In this work, we highlight how Compton scattering - i.e. inelastic scattering of photons by electrons [9] - can actually measure the number of electrons involved in hydrogen bonding, and we use this result to characterize structure and bonding in water under a variety of thermodynamical conditions. The Compton profile (CP) is given by

$$J(p, \mathbf{e}) = \int n(\mathbf{p}') \delta(\mathbf{p}' \cdot \mathbf{e} - p) d\mathbf{p}', \quad (1)$$

where  $\mathbf{e}$  is the unit vector along the scattering direction and  $n(\mathbf{p}')$  is the electron momentum density; here we only consider the spherical average  $J(p)$  over  $\mathbf{e}$ . The unique sensitivity of CPs to valence electrons and to chemical bonding (via  $n(\mathbf{p}')$ ) is at variance with diffraction techniques, which are principally sensitive to ionic positions. Earlier work using Compton scattering has in fact revealed the quantum nature of the hydrogen bond in ice [10], and it has also been suggested that CP can be a measure of the amount of H-bonding in water [11, 12, 13, 14, 15, 16, 17]. The Compton profile reflects the distribution of electronic momentum in the ground state of the measured system. Changes in bonding induce changes in this distribution and by tracking these changes both in experiment and calculations for water we establish two central points. First, we show that we can measure directly the number of electrons associated with change in bonding induced by varying thermodynamic

conditions. Then, we demonstrate a very robust linear relationship between  $n_{HB}$  and  $n_e$ , the number of electrons per molecule involved in hydrogen bonding, from ambient to supercritical conditions. Therefore, the measured  $n_e$  becomes a direct and unambiguous measure of  $n_{HB}$ .

As shown in Fig 1, our measurements cover the temperature range along the isobar  $P=300$  bar, and include the following state points: (a)  $T = 30$  °C (density =  $1.01$  g/cm<sup>3</sup>), liquid water reference; (b)  $T = 200$  °C (density =  $0.89$  g/cm<sup>3</sup>),  $T = 300$  °C (density =  $0.76$  g/cm<sup>3</sup>) and  $T = 350$  °C (density =  $0.67$  g/cm<sup>3</sup>), all showing precursor effects of hydrogen-bond breaking and change of local tetrahedral structure; (c)  $T = 397$  °C (density =  $0.40$  g/cm<sup>3</sup>), critical point neighborhood; (d)  $T = 416$  °C (density =  $0.21$  g/cm<sup>3</sup>), supercritical conditions.

Our measurements were taken at the European Synchrotron Radiation Facility in Grenoble at beamline ID15B using the 56 keV experimental set-up and a specially designed high-pressure cell [18]. The scattering angle was set at  $144.4^\circ$  and the back-scattered photons for the CP were collected by a Ge multi-element detector. After subtracting the very weak background ( $5 \times 10^{-3}\%$  at the Compton peak), the raw data were converted from wavelength scale to momentum scale, and multiple scattering contributions were subtracted from the measured profile in order to obtain the total profile. The multiple scattering contributions were calculated using Monte-Carlo simulations with each dataset treated separately in order to account the change in density. The ratio of multiple scattering to the total ranges between 0.9% at 30 °C to 5% at 416 °C. Our statistics ranges between  $2.1 \times 10^6$  counts at 30 °C to  $1.3 \times 10^6$  counts at 416 °C at the Compton peak. The energy-dependent resolution function was obtained from the full-width at half maximum of the elastic peak (0.51 atomic units of momentum). Now, since the CP is a projection of the electronic momentum density, its integral yields the total number of electrons and provides a convenient normalization. In this work, we focus our attention on CP differences, which are free from background contributions as long as the sample environment is unchanged. We limit ourselves to the stated thermodynamic range because measuring the CP of monomers (coordination 0) is not possible with the required high statistics and measuring ice Ih (coordination 4) would require a different sample environment. We thus present our data as the difference  $\Delta J(p)$  between a reference state CP (taken as liquid water at 30 °C and 300 bar) minus the CPs at higher temperatures. The acquisition times are of several hours.

Our Compton scattering calculations rely on first-principles methods without any struc-

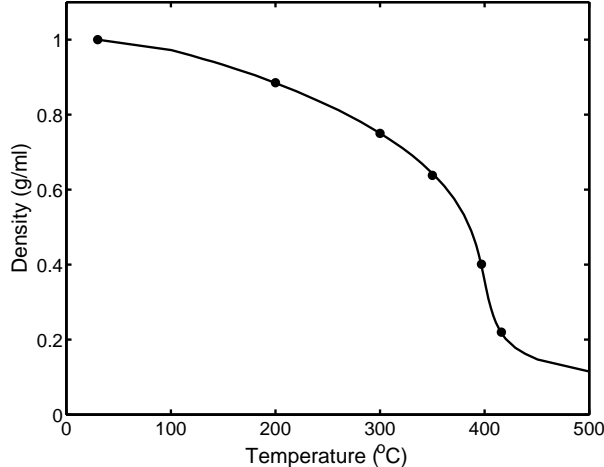


FIG. 1: Experimental measurements were taken along the isobaric curve for  $P=300$  bar.

tural information from experimental data (except for the density) [19]. To compare experiments with theory, we use extensive Car-Parrinello molecular-dynamics simulations [20, 21, 22], using 32 water molecules in periodic-boundary conditions. The subtle technical issues arising in the simulations of liquid water have been discussed extensively in the literature [23, 24, 25, 26] - in particular it has been suggested [27] that a closer agreement with experiments is obtained by constraining the internal degrees of freedom (i.e. keeping each water molecule rigid), given that at the conditions considered those vibrational degrees of freedom are frozen out and consequently in their zero-point motion state. We thus performed first-principles molecular-dynamics simulations at ambient, subcritical and supercritical regimes at 77, 200, 300, 350, 397 and 430 °C [28] with rigid water molecules. To determine the average water molecular structure to be used in the simulations mentioned above and to understand the effects of the change in intramolecular geometries on CP differences at various conditions, we also performed fully unconstrained Car-Parrinello molecular dynamics simulations [29]. These unconstrained simulations will also be used later to further confirm the linear relationship of  $n_e$  with  $n_{HB}$ . We further choose for the rigid-water molecular structure the average intramolecular O-H distance ( $r_{OH}$ ) and H-O-H angle ( $\angle_{HOH}$ ) to be 0.995 Å and 105.0° respectively, which are obtained from the 300 °C simulation. We note as expected in our unconstrained simulations, a small change in average structure over the range of temperatures considered, with  $r_{OH}$  and  $\angle_{HOH}$  varying between 104.6 - 106.1° and 0.990 - 0.998 Å respectively, when the temperature decreases

from 430 to 127 °C. These changes have, in principle, an effect on the CPs, but it will be shown that this effect is reduced to that of a scale factor: the linear relation alluded to above remains robustly verified. All our simulations were done in the NVT ensemble, with the densities fixed at the experimental values at 300 bar [30], using ultrasoft pseudopotentials with a plane-wave kinetic energy cutoff of 25 Ry for the wavefunctions and 200 Ry for the charge density. The wavefunction fictitious mass is chosen to be 1100 a.u. and a time step of 10 a.u. is used to integrate the electronic and ionic equations of motions. It is important to stress that these choices of fictitious mass and time step are the same as those used in Ref. [27], and are accurate for this system and wavefunction cutoff - i.e. they provide a structure that is not affected by integration errors. We note that fully-flexible water molecules described with norm-conserving pseudopotentials would require smaller fictitious masses ( $\sim 340$  a.u.) to provide accurate results - larger values will integrate less accurately the equations of motion, and lead to less structured radial distribution functions as compared to tightly-controlled simulations (such choices improve rather artificially the agreement with experiments, and lower the theoretical freezing point of water) [23].

The theoretical reference state is chosen to be that at 77 °C; a lower temperature would see the onset of a freezing transition [27]. The reason for the shift of the liquid-solid phase boundary have been discussed extensively in the literature [23, 24, 25, 27]; increasing the temperature for the only case (30 °C) close to the liquid-solid phase transition avoids the pitfall of remaining trapped in a glassy configuration. As a validation of the theoretical temperature scale, we found good agreement between the predicted and the measured self-diffusion coefficients. The predicted (and, in parenthesis, measured [31, 32]) self-diffusion coefficients obtained for water at 77 (30 in the experiment), 200, 300, 350, 397 and 430 °C are 1.5 (2.6), 9.5 (18.9), 27.0 (37.4), 35.3 (45.3), 75.9 (80.3) and 163.3 (174.4)  $\times 10^{-5} \text{cm}^2/\text{s}$ , respectively. We therefore adopt liquid (rigid) water at 77 °C, as a theoretical counterpart for the experimental temperature of 30 °C since the lowest temperature for which dynamics of water remains in the liquid phase is about 50 °C.

To compute  $J(p, \mathbf{e})$ , we used the approach by Romero *et al.* [33], based on maximally-localized Wannier functions [34]. Each water simulation lasted about 17 ps after thermalization, and at each temperature the CPs are calculated from the averages of 10 uncorrelated configurations, equally-spaced by 1.7 ps and then spherically averaged. The CPs are also convoluted with a Gaussian that matches the 0.51 a.u. experimental resolution.

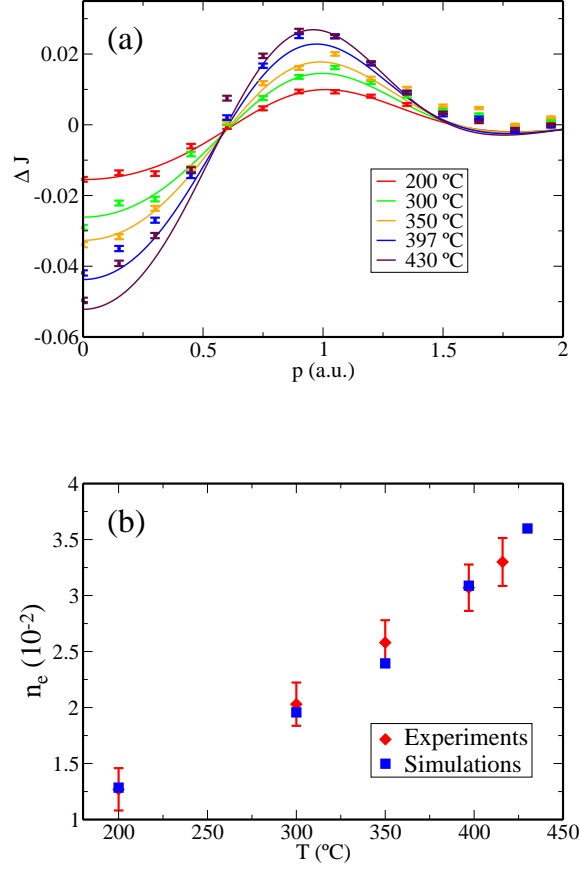


FIG. 2: (color online). (a) Experimental CP difference  $\Delta J(p)$  (points, in electrons per atomic unit of momentum) with respect to the experimental reference state as a function of temperature, and theoretical CP difference  $\Delta J(p)$  (solid lines, in electrons per atomic unit of momentum) with respect to the theoretical reference state as a function of temperature, and scaled by 0.73. The temperature of reference state is 30 °C for the experiments, 77 °C for the theory (at a density 0.97 g/cm<sup>3</sup>). For the purple experimental points the temperature is 416 °C while for the purple theory curve  $T = 430$  °C. (b) The number of electrons  $n_e$  involved in hydrogen bonding (i.e. integrated absolute profile difference) as a function of temperature (simulations have been scaled by 0.73).

We first show the experimental and theoretical  $\Delta J(p)$  in Fig. 2(a). The overall agreement between experiment and theory is excellent, provided the theoretical curves are rescaled to compensate for a systematic overestimation of the experimental values. The reasons for this overestimation can be manifold; they have been already reported in the literature [10, 12, 33], but will be discussed in detail later in this paper. What should be stressed however is that

a *unique* rescaling factor (here, 0.73) brings all theoretical curves in quantitative agreement with experiment.

We now propose an electronic measure of hydrogen-bonding defined by the number of electrons

$$n_e = \frac{1}{2} \int_{-\infty}^{\infty} |\Delta J(p)| dp, \quad (2)$$

where, as mentioned before,  $\Delta J(p)$  is the difference between the CPs at the conditions studied and the reference profile for normal liquid water. The area  $n_e$  (in units of electrons) between a difference curve and the horizontal axis in Fig. 2 measures the amount of electrons whose wavefunctions change in going from the reference state to the one being measured. The quantity  $n_e$  tracks the progressive breaking of hydrogen bonds as the temperature is raised from ambient conditions. Both the experimental measurements for  $n_e$  and the theoretical predictions (after rescaling) are plotted in Fig. 2(b) as a function of temperature. All the  $n_e(T)$  points line up, reflecting the agreement between the experimental and theoretical  $\Delta J(p)$  in Fig. 2(a). Interestingly,  $n_e(T)$  in Fig. 2(b) does not saturate, indicating that even at the highest temperatures considered significant hydrogen bonding remains. Moreover, the almost linear behavior of  $n_e(T)$  in the range from 200 to 430 °C mirrors a similar trend for  $n_{HB}$ , as shown in Ref. [2] (Fig. 13).

These considerations link  $n_e$  to the variation in hydrogen bonding as the temperature of the system is changed. In the following, we make a direct connection between  $n_e$  and  $n_{HB}$  by studying a model cluster where these quantities are unambiguous: a five-molecule model with one molecule at the center and the other four surrounding it in a tetrahedral arrangement. The O-O distance between two water molecules in the cluster geometry is fixed at 2.77 Å, which is the first peak height position of the theoretical O-O radial distribution function of liquid water at ambient conditions within our rigid water simulations. It has been shown [16] that the CP differences are strongly dependent on the O-O distance. An increase in the O-O distance will lead to a decrease in  $n_e$  and this can affect the scaling factor, as we shall discuss later in the paper. In the present cluster model, a single hydrogen bond can be formed or broken simply by removing, one at a time, the four outer molecules. This model was introduced in Ref. [14], but here, using maximally-localized Wannier functions [34], we can resolve the CP unique to the central molecule, as the hydrogen bonds with its neighbors are broken, one at a time. The number  $n_{HB}$  of hydrogen bonds formed by the central molecule is unambiguously defined, and the corresponding CP has been calculated

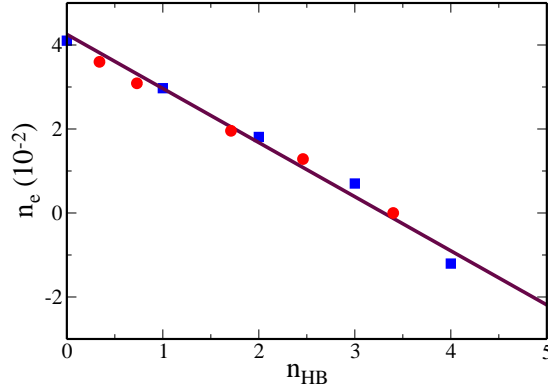


FIG. 3: (color online). The number of electrons  $n_e$  involved in hydrogen bonding (scaled by 0.73) as a function of hydrogen bonds  $n_{HB}$ . The zero on the vertical scale corresponds to the reference state at ambient conditions. Squares: water clusters (1 to 5 molecules); circles: rigid-water bulk simulations.

by averaging over all the possible clusters with a given  $n_{HB}$ .  $n_e$  can thus be plotted as a function of  $n_{HB}$ . The results are shown in Fig. 3 (squares), where  $n_e$  is again rescaled by a factor of 0.73, to facilitate a later connection with experiments. A linear dependence for the cluster results is seen and the slope provides an indication of the number of electrons involved in one hydrogen bond [35].

Finally, our first-principles molecular dynamics results are also plotted on Fig. 3, using for  $n_{HB}$  the structural definition [36] based on bond-length and bond-angle criteria. The  $(n_e, n_{HB})$  points collapse on the same straight line, confirming a universal relationship between  $n_e$  and  $n_{HB}$ , and demonstrating that the criteria [36] are meaningful and consistent with the natural integer  $n_{HB}$  count of the cluster model. Remarkably, the linear relationship between  $n_e$  and  $n_{HB}$  persists under a wide variety of conditions, ranging from the normal to the supercritical regime and covering all degrees of hydrogen bonding. Moreover, the slope in Fig. 3, as mentioned earlier, provides the number of electrons involved in a hydrogen bond:  $(13 \pm 0.6) \times 10^{-3}$  electrons are displaced for every bond that is broken (or formed). The bonding and coordination picture that emerges from these results is also in close agreement with the established understanding of coordination in liquid water. Our results are summarized in Table I, where we can see that in going from the normal state into the supercritical regime,  $n_{HB}$  decreases from 3.40 (compared to the value 3.58 from



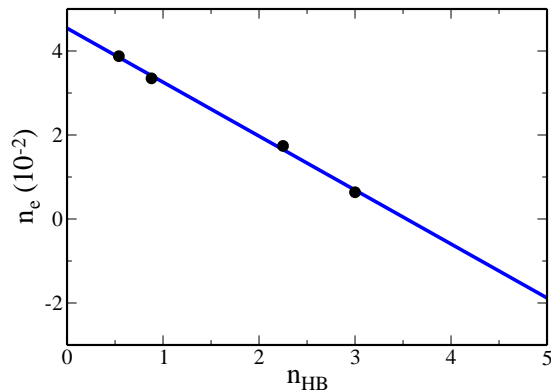


FIG. 4: (color online). The (unscaled) number of electrons  $n_e$  involved in hydrogen bonding as a function of hydrogen bonds  $n_{HB}$  for flexible water simulations at 200, 300, 403 and 430 °C. Note that the reference state in these calculations is 127 °C due to freezing at lower temperatures [23, 24, 25].

Ref. [6]) to 0.34. Moreover, except at ambient conditions, the theoretical  $n_{HB}$ 's at different temperatures agree reasonably well with the NMR studies [2], which also suggests that the simulations and experiments produce similar structures at the same temperatures above the theoretical melting point.

We now tackle in detail the origin of the rescaling factor. In principle, it is possible to exactly reproduce the amplitudes of the experimental CP differences by adjusting the intramolecular O-H distance and the H-bond geometry; this was detailed in Refs. [16] and [17]. Our approach uses instead geometries that are obtained directly from first-principles simulations and identifies a-posteriori the rescaling factor that aligns experiments and simulations. Note also that the proton zero-point motion is not accounted in any these simulations and may have a similar impact as discussed by Isaacs *et al.* [10] for the CP anisotropy of ice (the phenomenological rescaling used in those calculations was 0.6). For this same system, Romero *et al.* [33] have shown that finite temperature effects can be ruled out as the reason for rescaling and Ragot *et al.* [12] demonstrated that correlations effects are also not crucial. It is beyond the scope of this work to determine whether the proton zero-point motion or the difference in geometries due to the approximate exchange-correlation functionals dominate the discrepancies between experiments and theory. Instead, we show that the linear relation between  $n_e$  and  $n_{HB}$  holds even when intramolecular distances are allowed to change with

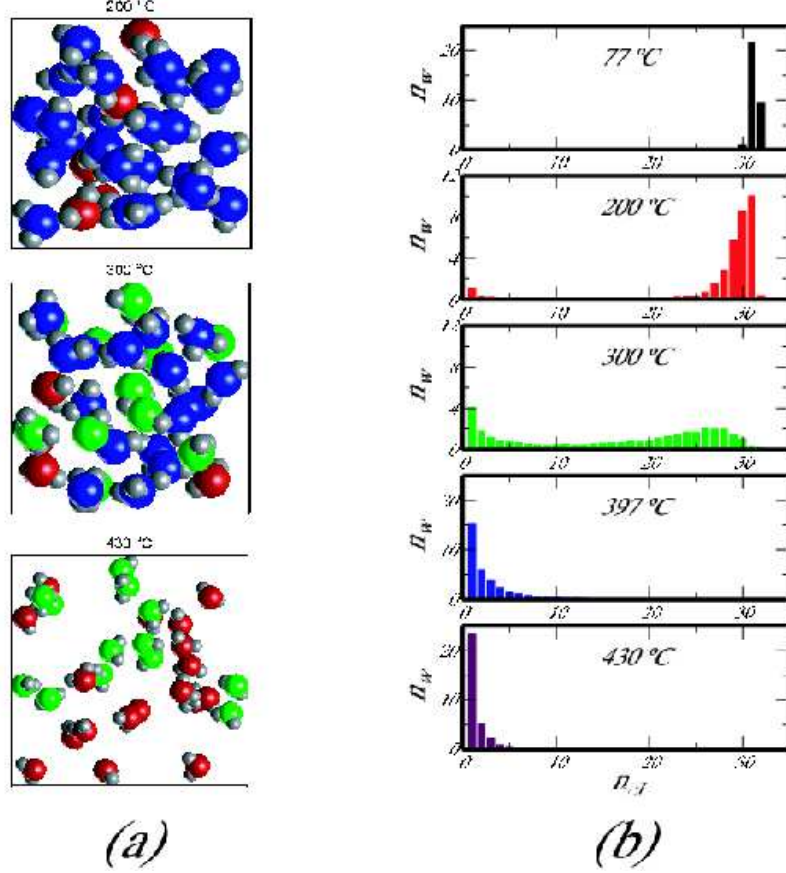


FIG. 5: (color online). (a) Snapshots from the simulations at 200 °C, 300 °C and 430 °C. Each panel shows the 32 inequivalent molecules in the periodic cubic supercell (note that the volumes at these conditions are very different, and the figures presented here have been rescaled accordingly). The color codes the connectivity of each water molecule (see text). Blue: water molecules in clusters with 6 or more molecules; green: water molecules in clusters with 2 to 5 molecules; red: monomers. (b) Number of water molecules  $n_w$  that belong to a cluster of size  $n_{cl}$ , at different temperatures.

temperature in fully unconstrained simulations. Even though these simulations are closer to the experiment as far as scaling is concerned we prefer to use the rescaled rigid water calculations for the fundamental reasons given above. Fig. 3 and Fig. 4 clearly show the remarkable robustness of our linear relation. Finally our fully unconstrained simulations clearly show that Compton profiles may be affected by changes in internal molecular geometry, but these changes are caused by hydrogen bonding and cannot be treated in a separate way.

We now examine the connectivity of the hydrogen-bond network as we move from the normal to the supercritical regime. For each molecule, we can determine the number of neighbors on a connected hydrogen-bond network. Fig. 5(a) shows three snapshots taken from our rigid water simulations. We see that at 200 °C most molecules (in blue) are in clusters containing 6 or more molecules, and very few monomers (in red) exist. Most remarkably, no intermediate cluster size exist - i.e. a molecule is either fully connected to all other, or fully disconnected, probably reminiscent of the very high surface tension of water. At 300 °C, there is a very wide distribution of cluster sizes: monomers and small clusters containing 2 to 5 molecules (in green). Finally, at 430 °C monomers dominate, but a few clusters of less than 6 molecules persist. To quantify these observations, we show in Fig. 5(b) the distribution of cluster sizes at a given simulation -  $n_w$  molecules belong to a cluster (of size  $n_{cl}$ ) if they are hydrogen bonded together. The uppermost panel of Fig. 5(b) shows that at normal conditions almost all water molecules are connected to each other. The percolating hydrogen-bond network breaks somewhere between 300 °C and 397 °C, as illustrated in Fig. 5(b) by the diffuse and bimodal distribution at 300 °C and the peaked, monotonically decreasing distribution at 397 °C. According to Table I, this is consistent with the well-known percolation threshold  $n_{HB} = 1.53 - 1.55$  [37]. Finally, the lowest panel in Fig 5(b) shows a distribution at 430 °C with a dominating amount of monomers but also a substantial amount of dimers and trimers, indicating that the amount of hydrogen bonds is still non-negligible in supercritical conditions. The experiment yields  $n_{HB}=0.74\pm0.16$  at 416 °C, while the simulation predicts  $n_{HB}=0.34$  at 430 °C. These values are consistent with Fig. 13 in the review article by Kalinichev [2].

In conclusion, we have shown that Compton scattering provides an absolute measure of the number  $n_e$  of electrons per water molecule involved in hydrogen bonds. We have measured the dependence of  $n_e$  as a function of temperature and compared with state-of-the-art first-principles molecular dynamics simulations. This comparison leads to a linear relation between  $n_e$  and the average number  $n_{HB}$  of hydrogen bonds per water molecule. The linear relation is very robust and holds over all possible coordination numbers. This approach should prove valuable in the future to address issues that arise in the characterization of hydrogen-bonded networks.

We acknowledge useful discussions with G. Loupias and V. Honkimaki, and thank B. Wood for his help and suggestions in calculating the connectivity of a bonding network. We

TABLE I: Experimental and theoretical (scaled by 0.73)  $n_e$ , and theoretical  $n_{HB}$  at different state points.  $n_{HB}$  is calculated from the molecular dynamics trajectories using the structural criterion of Ref. [3]. The first column shows the experimental temperature and pressure at each state point.

Temperature and pressure	$n_e$ ( $10^{-2}$ ) (experiment)	$n_e$ ( $10^{-2}$ ) (theory)	$n_{HB}$ (theory)
200 °C, 300 bar	$1.27 \pm 0.19$	1.28	2.46
300 °C, 300 bar	$2.03 \pm 0.19$	1.96	1.71
350 °C, 300 bar	$2.58 \pm 0.20$	2.39	1.38
397 °C, 300 bar	$3.07 \pm 0.21$	3.09	0.73
416 °C, 300 bar	$3.30 \pm 0.21$		
430 °C, 300 bar		3.60	0.34

also acknowledge support from the Croucher Foundation (P.H.-L.S.), MURI grant DAAD 19-03-1-0169 (N.M.), the MRSEC Program of the National Science Foundation under the award number DMR 02-13282 (P.H.-L.S.) and U.S.D.O.E. contracts DE-AC03-76SF00098, DE-FG02-07ER46352 (B.B.). The calculations in this work have been performed using the Quantum-ESPRESSO package [38]. Computational facilities have been provided through NSF grant DMR-0414849 and PNNL grant EMSL-UP-9597 at MIT, and the Northeastern University’s Advanced Scientific Computation Center (ASCC).

- 
- [1] D. Eisenberg and W. Kauzmann, *The Structure and Properties of Water*, Oxford University Press (Oxford, 1969).
  - [2] A. G. Kalinichev, *Reviews in Mineralogy and Geochemistry* **42**, 83-129 (2001).
  - [3] Ph. Wernet, D. Nordlund, U. Bergmann, M. Cavalleri, M. Odelius, H. Ogasawara, L. A. Näslund, T. K. Hirsch, L. Ojamäe, P. Glatzel, L. G. M. Pettersson, and A. Nilsson, *Science* **304**, 995 (2004).
  - [4] J. D. Smith *et al.*, *Science* **306**, 851 (2004); A. Nilsson *et al.*, *Science* **308**, 793 (2005); J. D. Smith *et al.*, *Science* **308**, 793 (2005).
  - [5] D. Prendergast and G. Galli, *Phys. Rev. Lett.* **96**, 215502 (2006).

- [6] A. K. Soper, F. Bruni, and M. A. Ricci, *J. Chem. Phys.* **106**, 247 (1997).
- [7] Ph. Wernet, D. Testemale, J.-L. Hazemann, R. Argoud, P. Glatzel, L. G. M. Pettersson, A. Nilsson, and U. Bergmann, *J. Chem. Phys.* **123**, 154503 (2005).
- [8] M. V. Fernández-Serra and E. Artacho, *Phys. Rev. Lett.* **96**, 016404 (2006).
- [9] M.J. Cooper *et al.* in *X-Ray Compton Scattering*, Oxford University Press (2004).
- [10] E.D. Isaacs, A. Shukla, P. M. Platzman, D. R. Hamann, B. Barbiellini, and C. A. Tulk, *Phys. Rev. Lett.* **82**, 600 (1999).
- [11] T. K. Ghanty, V. N. Staroverov, P. R. Koren, and E. R. Davidson, *J. Am. Chem. Soc.* **122**, 1210 (2000).
- [12] S. Ragot, J.M. Gillet, and P.J. Becker, *Phys. Rev. B* **65**, 235115 (2002).
- [13] B. Barbiellini and A. Shukla, *Phys. Rev. B* **66**, 235101 (2002).
- [14] M. Hakala, S. Huotari, K. Hämäläinen, S. Manninen, Ph. Wernet, A. Nilsson, and L. G. M. Pettersson, *Phys. Rev. B* **70**, 125413 (2004).
- [15] M. Hakala, K. Nygard, S. Manninen, L. G. M. Pettersson, and K. Hämäläinen, *Phys. Rev. B* **73**, 035432 (2006).
- [16] M. Hakala, K. Nygard, S. Manninen, S. Huotari, T. Buslaps, A. Nilsson, L. G. M. Pettersson, and K. Hämäläinen *J. Chem. Phys.* **125**, 084504 (2006).
- [17] K. Nygard, M. Hakala, S. Manninen, A. Andrejczuk, M. Itou, Y. Sakurai, L. G. M. Pettersson, and K. Hämäläinen, *Phys. Rev. E* **74** 031503 (2006).
- [18] D. Testemale, R. Argoud, O. Geaymond, and J.-L. Hazemann, *Review of Scientific Instruments*, **76**, 043905 (2005).
- [19] While also the density could be determined fully from first-principles constant pressure simulations, the timescale needed for statistical accuracy are still beyond ordinary computer resources, especially in the supercritical regimes.
- [20] R. Car and M. Parrinello, *Phys. Rev. Lett.* **55**, 2471 (1985).
- [21] K. Laasonen, A. Pasquarello, R. Car, C. Lee, and D. Vanderbilt, *Phys. Rev. B* **47**, 10142 (1993).
- [22] D. Marx and J. Hutter, <http://www.fz-juelich.de/nic-series/Volume1/marx.pdf>
- [23] J. C. Grossman, E. Schwegler, E. W. Draeger, F. Gygi, and G. Galli, *J. Chem. Phys.* **120**, 300 (2004).
- [24] E. Schwegler, J. C. Grossman, F. Gygi, and G. Galli, *J. Chem. Phys.* **121**, 5400 (2004).

- [25] P. H.-L. Sit and N. Marzari, J. Chem. Phys. **122**, 204510 (2005).
- [26] Joost VandeVondele, F. Mohamed, M. Krack, J. Hutter, M. Sprik, and M. Parrinello, J. Chem. Phys. **122**, 014515 (2005).
- [27] M. Allesch, E. Schwegler, F. Gygi, and G. Galli, J. Chem. Phys. **120**, 5192 (2004).
- [28] In all the molecular dynamics simulations, a Nose-Hoover thermostat is applied to the ions, but no electronic thermostat is used.
- [29] The details of simulations at ambient conditions can be found in Ref. [25]. We also performed simulations at 200, 300, 403 and 430 °C, all at 300 bar. Pseudopotentials, fictitious mass and timestep are the same as those used in Ref. [25]. Unlike the rigid water simulations, all the flexible water simulations were done with heavy water molecules.
- [30] At 77 °C, the density is taken to be that at 1 bar, and differs by less than 4% from the one at 300 bar.
- [31] W. J. Lamb, G. A. Hoffman, and J. Jonas, J. Chem. Phys. **74**, 6875 (1981).
- [32] K. Yoshida, C. Wakai, N. Matubayasi, and M. Nakahara, J. Chem. Phys. **123**, 164506 (2005).
- [33] A. H. Romero, P. L. Silvestrelli, and M. Parrinello, J. Chem Phys. **115**, 115 (2001).
- [34] N. Marzari and D. Vanderbilt, Phys. Rev. B **56**, 12847 (1997).
- [35] The negative value of  $n_e$  for  $n_{HB}=4$  is due to the fact that the definition of  $n_e$  should be generalized, when the reference state is less coordinated than the considered state, to  $n_e = \frac{-\Delta J(0)}{2|\Delta J(0)|} \int_{-\infty}^{\infty} |\Delta J(p)| dp$ .
- [36] We adopt the geometrical criterion for H-bond suggested in Ref. [3]. It is considered to be a hydrogen bond when  $r_{OO} \leq 3.3 \text{ \AA} - 0.00044\theta^2$ , where  $\theta$  is the H-bond O-H-O angle.  $\theta=0$  when the H-bond is linear.
- [37] R. L. Blumberg, H. E. Stanley, A. Geiger, and P. Mausbach, J. Chem. Phys. **80**, 5230 (1984).
- [38] S. Baroni *et al.*, <http://www.quantum-espresso.org>.